Experimental fault zone mechanics

Strain localization in granular fault zones at laboratory and tectonic scales

C. Marone & A.P. Rathbun
Department of Geosciences and Center for Geomechanics, Geofluids, and Geohazards, The Pennsylvania State University, University Park PA, USA

ABSTRACT: We present results from laboratory experiments and a numerical model for frictional weakening and shear localization. Experiments document strain localization in sheared layers at normal stresses of 0.5 to 5 MPa, layer thicknesses of 3 to 10 mm, and imposed slip velocities of 10 to 100 μm/s. Passive strain markers and the response to load perturbations indicate that the degree of shear localization increases for shear strains γ of $0.15 < \gamma < 1$. Our numerical model employs rate-state friction and uses 1D elasto-frictional coupling with radiation damping. We interrogate the model frictional behavior by imposing perturbations in shearing rate at the fault zone boundary. The spatial distribution of shear strain depends strongly on frictional behavior of surfaces within the shear zone. We discuss the onset of strain localization and the width of active shear strain for conditions relevant to earthquake faulting and landslides. state relevant to earthquake faulting and landslides.

1 INTRODUCTION

Laboratory and field evidence indicate that strain localization is accompanied by significant changes in hydraulic and mechanical properties of rocks (e.g., Wood 2002, Song et al., 2004, Rice 2006). Strain localization occurs at a broad range of scales and involves both formation of faults and, upon continued shear, confinement of shear to narrow bands within the wear and gouge materials that constitute the fault zone. Of particular interest is the connection between strain localization and the transition from stable to unstable frictional sliding within shear zones of finite width (e.g., Anand & Gu 2000, Rice & Cocco 2007).

2 SHEAR LOCALIZATION IN GRANULAR LAYERS

In this paper we focus on layers composed of granulated rock. Granular layers were sheared in a biaxial deformation apparatus using the double-direct shear configuration. Details of the testing apparatus and experimental procedures are reported in Rathbun et al. (2008). Layers were initially 3 to 10 mm-thick and we imposed slip velocities of 10 to 100 μm/s at the layer boundary. Normal stress was held constant during shear via a fast-acting servo-hydraulic control mechanism. We discuss experiments conducted at normal stresses in the range 0.5 to 5 MPa, which is high enough to result in inelastic yield at grain to grain contacts, on the upper end, and low enough to inhibit grain crushing, on the lower end.

2.1 *Dilation as a proxy for shear localization*

Previous studies of granular layers have established that upon shear loading, shear stress rises linearly before undergoing a progressive transition from elastic to inelastic behavior (e.g., Anthony & Marone 2005). Inelastic yield is associated with grain rearrangement, compaction, and bulk shear strain of the layer (e.g., Marone 1998). Figure 1 illustrates this behavior for a granular layer that was initially 10 mm thick and sheared at a normal stress of 1 MPa. Note the steep rise in shear stress followed by strain hardening and a transition to steady frictional sliding at a shear strain of ~0.5. Layers compact during the initial rise in shear stress and dilation beings at a normalized stress

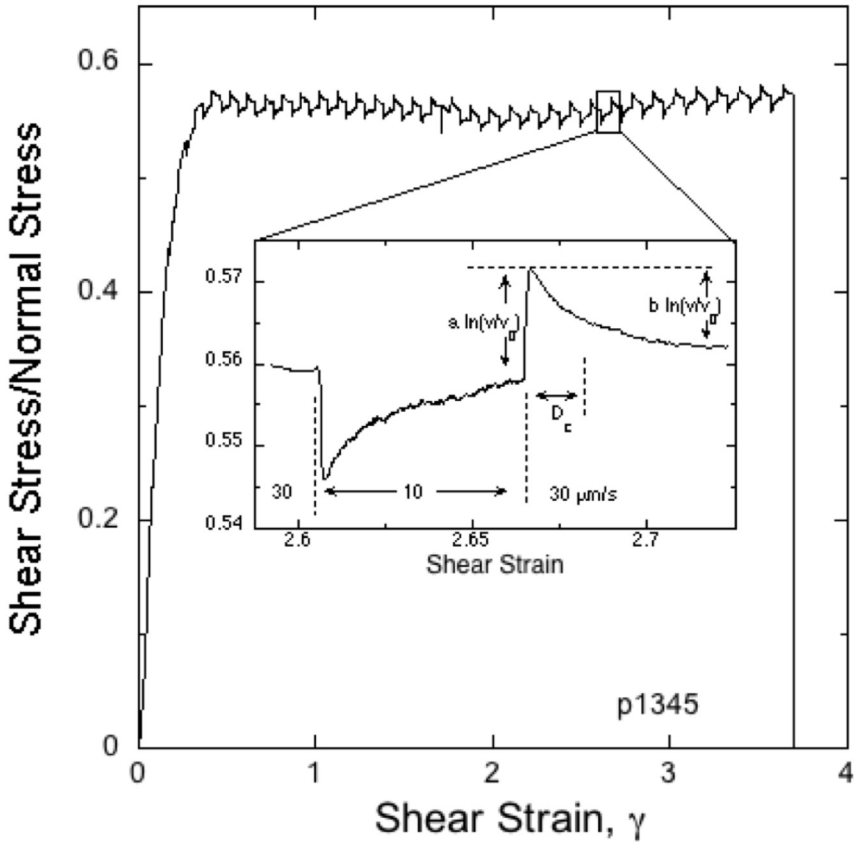

Figure 1. Complete stress-strain curve for a granular layer sheared at a 1 MPa normal stress. Initial layer thickness was 10 mm. Normalized shear stress is plotted versus engineering shear strain computed from incremental displacement at the layer boundary divided by instantaneous layer thickness. Note the steep, quasi-linear, initial rise in shear stress followed by hardening and fully-mobilized shear at strains of 0.4 to 0.5. Beginning at a shear stain of 0.3, the shearing rate at the layer boundary was toggled between 10 and 30 μm/s. Inset shows detail of the friction response to step changes in slip velocity. The material is glacial till, (Caesar till, Ohio, USA) which is a mixed-size granular material (Particle size D: $D_{max} = 1$ mm, D50 ∼0.3 mm, 90% of the particles >0.1 mm) similar to natural fault gouge (after Rathbun et al., 2008).

(friction) level of 0.35 to 0.4 (Fig. 1). In this experiment we evaluated the effects of changes in slip velocity at the layer boundary. The systematic variation in friction seen throughout the experiment is associated with step changes in loading rate between 10 and 30 μm/s, as discussed further below.

In granular layers, the transition from initial strain hardening to steady-state (fully mobilized) frictional sliding is associated with the development of localized shear (e.g., Logan et al., 1979, Marone et al., 1992). Recently, Rathbun et al. (2008) showed that stress perturbations, and layer dilation, provide a more precise measure of the degree of shear localization. They showed that small perturbations in the shear stress level during creep friction tests provide a proxy for shear localization (Fig. 2). Creep friction tests were carried out at a constant shear stress level below that for stable sliding. Using this approach, the degree of shear localization can be assessed with the parameter Δh^*, which is the layer dilation for a unit increase in shear stress. We measured Δh^* as a function of shear strain for a range of conditions (Fig. 2). Dilation scales with layer thickness below a critical value of shear strain. For shear strains $\leq \sim 0.5$, thicker layers exhibit larger values of Δh^* than thinner layers (Fig. 2). However for shear strains greater than ∼1, dilation is independent of layer thickness. These data show that, initially, shear is distributed across the full thickness of the

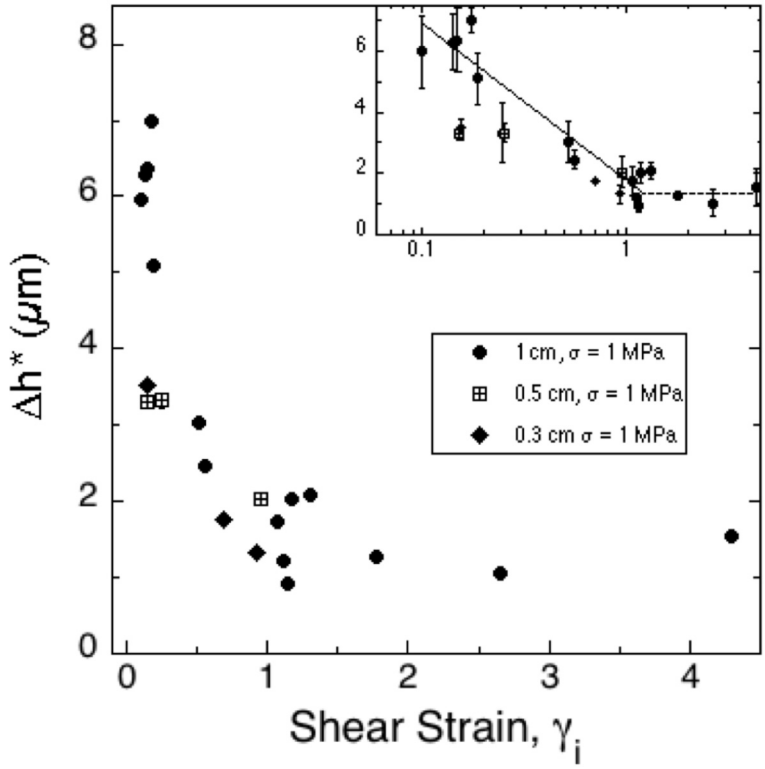

Figure 2. Data showing layer dilation Δh^*, used as a proxy for shear localization, as a function of shear strain. The parameter Δh^* is the layer dilation for an increase in shear stress equal to 5% of the strength during stable frictional sliding. Data are shown from multiple experiments with initial layer thicknesses ranging from 3 to 10 mm. Normal stress was 1 MPa in all cases. During steady-state frictional sliding, friction is typically 0.55 to 0.6 (e.g. Fig. 1); thus the shear stress perturbations were of order 0.03 MPa.

layer, but that shear becomes localized beyond a critical shear strain. The data of Figure 2 indicate that shear is fully localized by shear strains of roughly unity.

Figure 3 shows additional details of the relationship between shear stress, shear strain, and layer thickness. This figure shows stress-strain curves for representative experiments and one data set for changes in layer thickness as a function of shear strain (experiment p1025). Layer dilation occurs early in the strain history and then the layers compact slightly before reaching a steady level, consistent with a critical state, for shear strains of 0.3 and greater (Fig. 3).

2.2 *Rate/State friction and shear localization*

Slip velocity step tests have emerged as a powerful tool for interrogating friction constitutive behavior (Dieterich 1979, Ruina 1983, Scholz, 1998). A large body of literature shows that frictional strength of a wide range of materials exhibits two responses to a step increase in the imposed loading rate (e.g., Dieterich & Kilgore 1994, Tullis 1996, Marone 1998). First, there is an instantaneous change in frictional resistance of the same sign as the velocity change. This is referred to as the friction direct effect and it is described by the friction parameter a. Figure 4 defines the key parameters and outlines the rate and state friction equations. The direct effect is followed by a gradual evolution of strength, scaled by the friction parameter b (Fig. 4). The evolution effect is typically of the same as the change in velocity (Fig. 1). Existing studies show that the evolution effect occurs over a characteristic slip distance, D_c (sometimes referred to as L), for initially-bare solid surfaces or a characteristic strain for layers of granular/clay particles (e.g., Marone 1998).

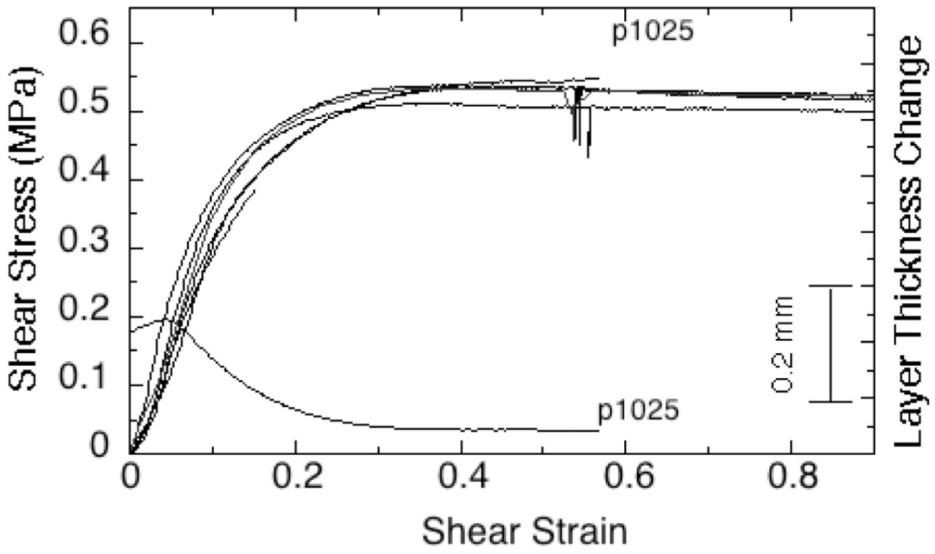

Figure 3. Complete stress strain curves for five experiments along with a representative data set (experiment p1025) for changes in layer thickness as a function of shear strain. The layer thickness started at 10 mm in experiment p1025 and the thickness was measured continuously during shear with a DCDT. Note that dilation occurs during the initial increase in stress but that compaction begins prior to fully-mobilized shear within the granular layer.

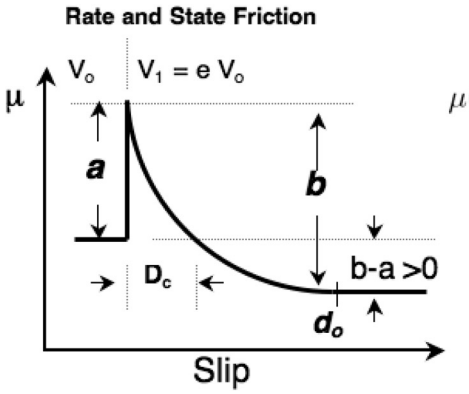

$$\mu(\theta, v) = \mu_o + a\, ln\left(\frac{v}{v_o}\right) + b\, ln\left(\frac{v_o\theta}{D_c}\right)$$

$$\frac{d\theta}{dt} = 1 - \frac{v\theta}{D_c}$$

$$\frac{d\mu}{dt} = k\,(v_{lp} - v)$$

Figure 4. The equations describing the rate and state friction constitutive law along with a schematic showing this behavior.

The values of D_c are typically larger for shear within a granular layer than for shear between solid surfaces (e.g., Marone & Kilgore 1993, Marone et al., 2009).

To the extent that the friction evolution effect is truly driven by shear displacement, step velocity increases and decreases are expected to yield symmetric behavior. Such symmetry was found by Ruina (1983) and Marone et al. (1990). Other studies have favored a model in which friction evolution occurs over a characteristic time (Beeler et al., 1994, Sleep 1997). Finally, a large number of works have evaluated only velocity increases or decreases, without considering the issue of symmetry (e.g., Marone & Kilgore 1993). Few studies have systematically evaluated symmetry of the friction response to changes in loading velocity.

2.3 *Mechanics of the critical slip distance for friction of granular materials*

For solid surfaces in contact, the critical slip distance for friction evolution can be thought of in terms of the asperity contact lifetime, given by the contact size divided by the average slip rate (Rabinowicz 1951, Dieterich 1979). When coupled with the adhesive theory of friction (e.g., Bowden & Tabor 1950), in which asperity strength (and size) is proportional to time of contact (lifetime), this model predicts that frictional strength during steady-sliding should decrease with increasing slip velocity, because contact lifetime (hence strength) is inversely proportional to sliding velocity. In the context of a velocity step test, the critical friction distance is the slip necessary to replace contacts with a lifetime given by the initial velocity by contacts corresponding to the final velocity (Dieterich 1979, Ruina 1983).

For granular materials the situation is slightly more complex. The model for solid friction can be applied directly for asperity contacts between grains. However, granular interactions and stress transmission via particle contacts lead to a second characteristic length scale, in addition to the asperity contact junction size. The work by Marone & Kilgore (1993) shows that the critical slip distance for granular shear depends on both the particle size and the shear localization dimension (Fig. 5).

The data of Figure 5 show measurements of the critical slip distance as a function of shear strain for granular layers sheared in the double-direct shear geometry. The average particle sizes ranged from 700 μm (Coarse) to 5 μm (Fine); fractal is a power-law size distribution between 45 and 720 μm. The critical slip distance is greatest for larger particles at all values of shear strain (Fig. 5). Fine particles, with an average size that is roughly 100 times smaller than the coarse

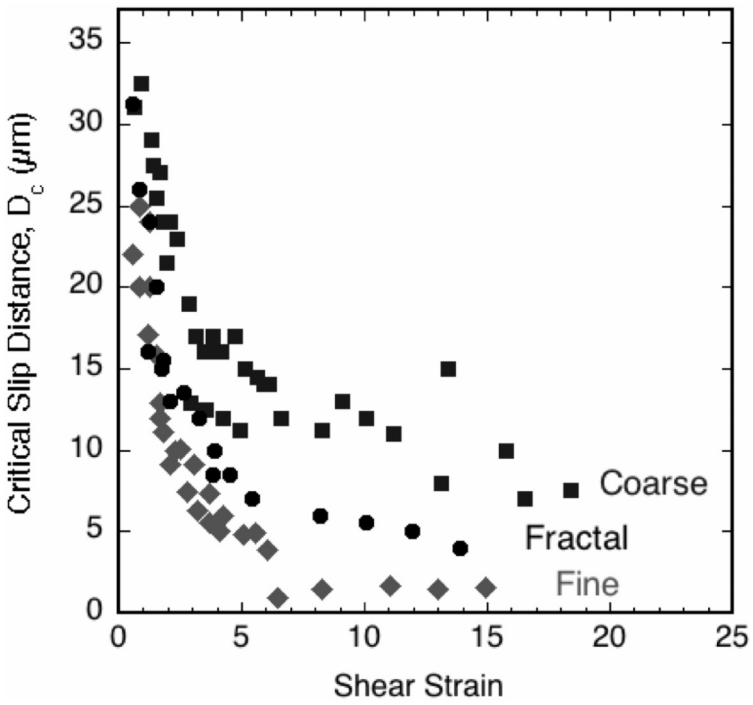

Figure 5. Measurements of the critical slip distance for granular layers as a function of shear strain. Data are shown for three particle size distributions. Note that the critical slip distance is greatest for larger particles at all values of shear strain. *Coarse*: Ottawa sand ASTM C-190 all particles are 600 to 800 μm. *Fine*: Silcosil 400 mesh (US Silica Co.) with median and maximum diameter of 1.4 and 10 μm, respectively. *Fractal*: given by $N(n) = bn^{-D}$, where $N(n)$ is the number of particles of size n, b is a constant and D is the fractal dimension 2.6, made using particles in the range <45 μm to 700 m. Data from Marone & Kilgore (1993).

particles, have a critical slip distance that is roughly 10 times smaller than the coarse particles, consistent with the expected scaling between contact junction dimension and particle diameter. It is important to note, however, that the difference in D_c values for coarse and fine particles is small compared to the observed evolution of D_c with shear strain (Fig. 5). The D_c values for layers of both coarse and fine particles decrease by more than 100% of the final value at shear strains greater than ∼7. The decrease in D_c with shear strain is consistent with the effects of shear localization.

2.4 *Observations of shear localization*

Laboratory investigations of shear localization often include post-experiment examination of preserved microstructures (e.g., Mair & Marone 1999). In the experiments described here, we used passive markers in some experiments to record the strain distribution across layers (Figure 6). The markers were constructed with blue sand grains. Following the shear experiment, layers were impregnated with epoxy and then cut parallel to the shear direction. Figure 6 shows a layer that was sheared, top to the left, to a strain of 3.9. The layer had three markers that were initially vertical in the orientation of the photograph. The original image is shown below a copy (above) that has been marked to highlight the offset marker. Note that: 1) the marker is offset primarily along a zone near the center of the layer and 2) that the segments above and below the primary offset show distinct curvature. This curvature indicates a progressive localization process prior to development of the main shear zone in the center of the layer. By measuring offset of the top and bottom limbs of the marker, we calculated a shear strain of 3.25 along the shear zone at the center of the layer. Based on the total shear strain of 3.9, we estimate initiation of this shear band at a shear strain of 0.65, which is within the range indicated by our layer dilation measurements (Fig. 2).

Figure 7 is a schematic illustration of two modes by which shear could become localized. In panels a–c the marker is first subject to uniform strain and then cut by a shear zone. In this scenario, shear localizes abruptly. The markers are first rotated by simple shear and then cut and offset along a narrow zone at the center of the layer. Panels d–f show a more progressive localization process (Fig. 7). The markers are initially subject to uniform strain, but localization occurs gradually and on several surfaces near the center of the zone. The markers are bent into an arcuate shape by progressively greater strain concentration with increasing distance from the layer boundaries (Fig. 7). Eventually, the strained markers are offset along a primary shear band. This type of localization process, with a gradual transition from pervasive to localized strain is consistent with our dilation measurements, which indicate progressively greater localization over the range of macroscopic shear strain from 0.15 to 1.0. Moreover, thin sections from our experiments (Fig. 6) indicate a progressive localization process, like panels d–f of Figure 7, rather than an abrupt transition.

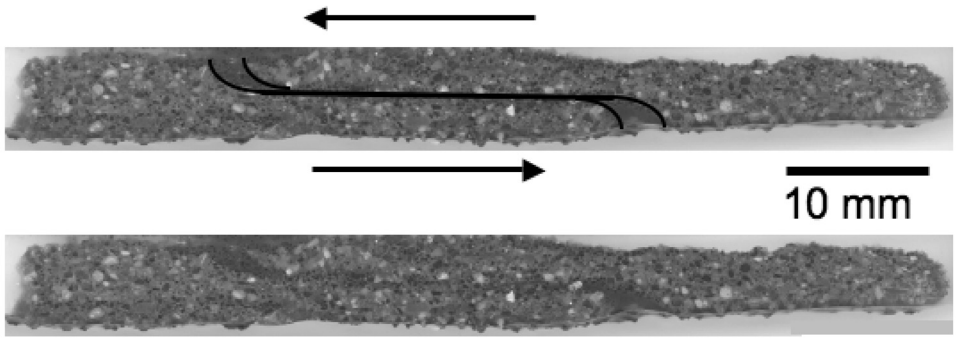

Figure 6. Thin section of a granular layer that was subject to a shear strain of 3.9. The layer contains three passive markers that were initially vertical, in this orientation, formed by darker particles. Top image is annotated to show shear of the central marker. Lower image is unmarked photograph.

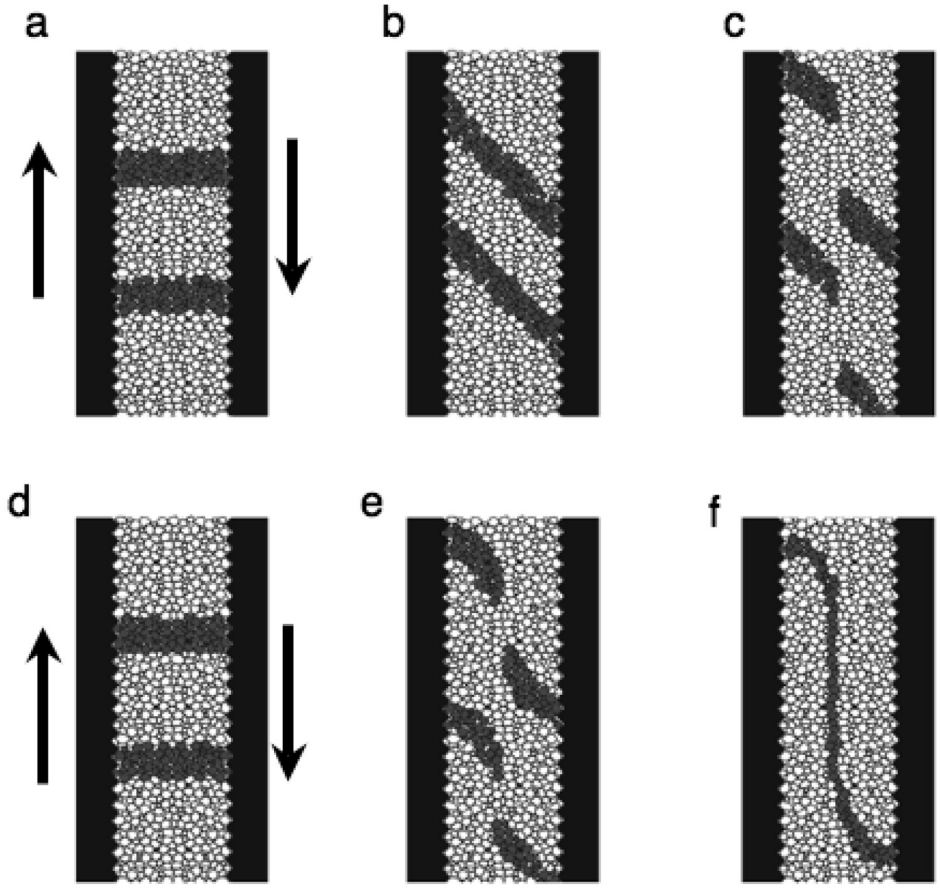

Figure 7. Schematic representations of two models for shear localization in a granular layer. Darker particles are passive markers. Panels a and d show initial, un-deformed state. Panels a–c show pervasive shear followed by abrupt shear localization. Panels d–f show progressive shear and localization. Strain is pervasive for the interval from panel d to panel e, but then shear localizes between e and f. Panel f shows one marker that is deformed and offset. Note similarity between panel f and micrograph in Figure 6.

3 A NUMERICAL MODEL FOR FRICTIONAL WEAKENING AND SHEAR LOCALIZATION

To address shear localization in tectonic fault zones and to improve our understanding of the scaling problem associated with applying laboratory observations to faults in Earth's crust, we employ a numerical model. The model describes frictional shear in a fault zone composed of multiple, parallel surfaces that obey rate and state friction (Fig. 8). The model used here is based on that described by Marone et al. (2009). We extend that model and focus on coupling between friction properties and shear localization.

3.1 *Elasto-frictional model for a fault zone of finite thickness*

A typical tectonic fault zone consists of a highly damaged zone surrounded by progressively less damaged country rock (e.g., Chester & Chester 1998). Thus, in the context of the seismic cycle, the zone of slip deformation is defined by a critical fracture density, above which slip and deformation occurs, and below which the rock behaves as intact material. One could imagine a model in which

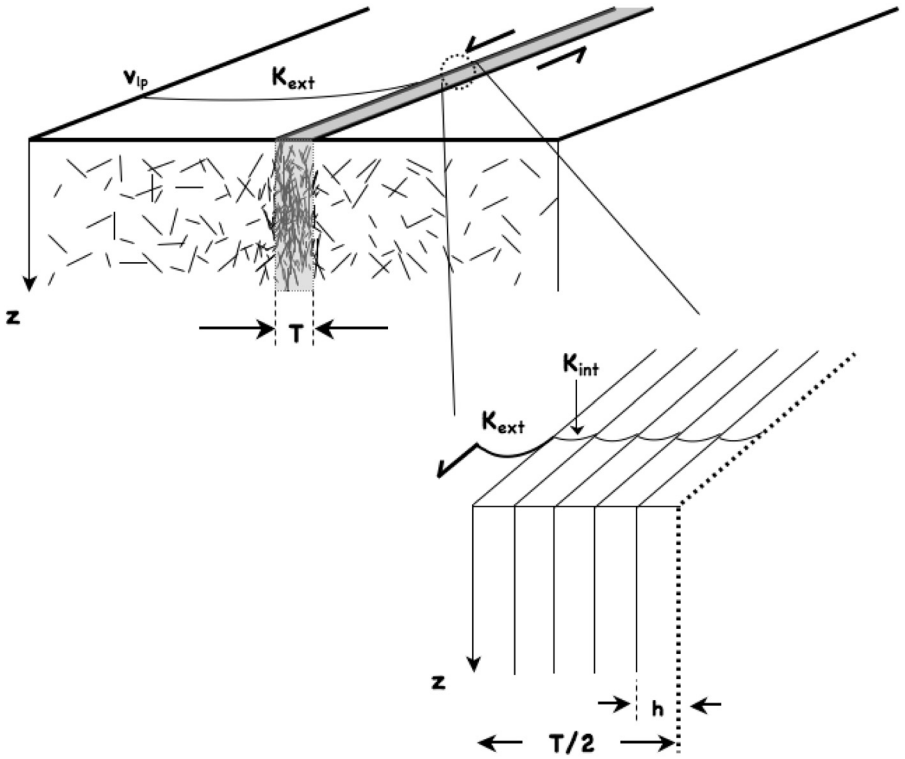

Figure 8. Fault zone model and schematic of shear zone composed of multiple sub-parallel surfaces. The fault zone width is T. K_{ext} represents elastic stiffness of the crust surrounding the fault. K_{int} represents elastic coupling between surfaces in the model, which are separated by distance h. The model is symmetric about the center.

this critical fracture density depended on strain rate and other factors, such that the effective fault zone width varied throughout the seismic cycle, but we make the simplifying assumption of constant width T (Fig. 8).

Within the model fault zone, shear may occur on one or more sub-parallel surfaces (Fig. 8). Our aim is to investigate spatio-temporal complexity of shear localization in a fault zone that experiences a rapid change in imposed slip rate; for example due to earthquake propagation into the region of interest. Therefore we employ a simplistic geometry and elastic model. As an initial condition, we assume homogeneous creep within the fault zone, such that all surfaces are slipping at a background rate. We investigate the fault response to perturbations in slip rate imposed at the fault zone boundary at $\pm T/2$ relative to the center of the zone (Fig. 8).

Potential slip surfaces within the fault zone interact via elasto-frictional coupling. Stress is transmitted between surfaces only when: 1) the frictional strength of a surface exceeds the current stress level, or 2) a surface slips and its strength changes. In the models described here, stresses and frictional strengths are initially equal on all surfaces. Slip surfaces obey laboratory-based rate and state friction laws, and we focus here on the case of state evolution via the Ruina law (Dieterich 1979, Ruina 1983). A one-dimensional elastic model is used with radiation damping to solve the equations of motion.

Each surface i in the model shear zone obeys rate and state frictional behavior, such that friction μ_i is a function of state θ_i and slip velocity v_i according to:

$$\mu_i(\theta_i, v_i) = \mu_0 + a \ln\left(\frac{v_i}{v_0}\right) + b \ln\left(\frac{v_0 \theta_i}{L}\right) \tag{1}$$

Table 1. Model parameters. For all cases, $G = 30$ GPa, $\sigma = 100$ MPa, $K_{\text{int}} = G/h; K_{\text{int}}/K_{\text{ext}} = 10$; $v_o =$ 1e-6 m. $n_s/2$ is the number of surfaces in the fault zone half width $T/2$.

a	b	L (m)	h (m)	K_{ext}/σ_n (m^{-1})	$n_s/2$	T (m)	v (m/s)
0.012	0.016	1e-5	6e-3	5e4	30	0.60	0.01

where μ_0 is a reference friction value at slip velocity v_0, and the parameters a, b, and L are empirically-derived friction constitutive parameters (e.g., Marone 1998). Note that we use L for the model critical slip distance, rather than D_c, which is the effective parameter measured from laboratory experiments. Tectonic fault zones are likely to include spatial variations of the friction constitutive parameters within the shear zone, and thus we allow such behaviors.

The model includes n_s parallel surfaces, where $i = 0$ is at the fault zone boundary. Surfaces are coupled elastically to their neighbors via stiffness K_{int}. We assume $K_{\text{int}} = G/h$, where G is shear modulus and h is layer spacing (Fig. 8) and use $G = 30$ GPa. We assume that remote tectonic loading of the shear zone boundary is compliant relative to K_{int} and take $K_{\text{int}}/K_{\text{ext}}$ equal to 10.0. This is equivalent to assuming a constant spacing between surfaces and means that wider shear zones, with more internal surfaces, are effectively more compliant than narrower zones. Another approach would be to take $K_{\text{int}}/K_{\text{ext}}$ equal to the number of surfaces in the shear zone. Details of the parameters used are report in Table 1.

We analyze friction state evolution according to:

$$\frac{d\theta_i}{dt} = -\frac{v_i\theta_i}{L}\ln\left(\frac{v_i\theta_i}{L}\right) \text{ (Ruina Law)} \tag{2}$$

Frictional slip on each surface satisfies the quasi-dynamic equation of motion with radiation damping (Rice 1993):

$$\mu_i = \frac{\tau_0}{\sigma_n} - \frac{G}{2\beta\sigma_n}(v_i - v_{pl}) + k(v_{pl}t - v_i t) \tag{3}$$

where μ_i is the frictional stress, τ_0 is an initial stress, β is shear wave speed, σ_n is normal stress, k is stiffness divided by normal stress, and t is time. Differentiating Equations 1 and 3 with respect to time and solving for dv_i/dt yields:

$$\frac{dv_i}{dt} = \frac{k(v_{pl} - v_i) - b\frac{d\theta_i}{dt}}{\frac{a}{v_i} + \frac{G}{2\beta\sigma_n}}, \tag{4}$$

which applies for each surface within the shear zone. Our approach for including radiation damping is similar to that described in previous works (Perfettini & Avouac 2004, Ziv 2007).

We assume that the model begins with steady creep, and thus each surface of the fault zone undergoes steady state slip at velocity $v_i = v_0$ with $\mu_0 = 0.6$ and $\theta_{ss} = L/v_0$. The effective stiffness k_i between the load point and surface i within the fault zone is given by:

$$\frac{1}{k_i} = \frac{1}{K_{\text{ext}}} + \sum_{j=1}^{i}\frac{1}{K_{\text{int}_j}}. \tag{5}$$

To determine shear motion within the fault zone, we solve the coupled Equations 2, 4–5, using a 4th order Runga-Kutta numerical scheme. As noted above, perturbations in slip velocity are imposed at the shear zone boundary. This is assumed to occur via a remote loading stiffness K_{ext}.

Then, for each time step in the calculation, the surface with the lowest frictional strength is allowed to slip.

Our initial conditions are that shear and normal stress are the same on each surface. We ensure that time steps are small compared to the ratio of slip surface separation, h, to elastic wave speed. Thus, within a given time step, only one surface slips and it is coupled elastically to the remote loading velocity via the spring stiffness given in Equation 5.

3.2 *Frictional response to changes in imposed slip rate*

Figure 9 shows macroscopic shear strength of the fault zone as a function of slip at the fault zone boundary. Shear stresses are equal on all slip surfaces, however frictional strengths are not. Thus, Figure 9 shows friction of the weakest surface within the fault zone as a function of offset at the fault zone boundary. This case shows behavior of a fault zone that has homogeneous frictional properties.

The macroscopic frictional response of the fault zone differs from the constitutive response of the individual surfaces within it. In particular, the fault zone exhibits a protracted phase of strain hardening prior to reaching the maximum yield strength (Fig. 9). The peak strength is reached in a slip displacement of $<5\%$ of D_c for a single surface, whereas the fault as a whole requires slip equal to 200% of D_c before weakening begins. As a result, the effective critical friction distance for the fault zone significantly exceeds that for an individual slip surface (Fig. 9). The maximum yield strength of the fault zone, which is proportional to the friction parameter a, is nearly identical to that for an individual surface. Finally, the steady-state frictional strength is the same in both cases (Fig. 9).

The relationship between the intrinsic frictional behavior of a surface and the zone of active shear, as a whole, is important for several aspects of earthquake rupture and shear localization. Figure 10 shows this relationship for a series of model runs to different shear strains. In each case the intrinsic frictional response of a single surface is shown versus slip on that surface. In addition, the frictional strength for the shear zone is plotted versus boundary slip. The two curves are plotted on the same scale; but note that the single surface is subject to larger total slip displacement, so as to illustrate

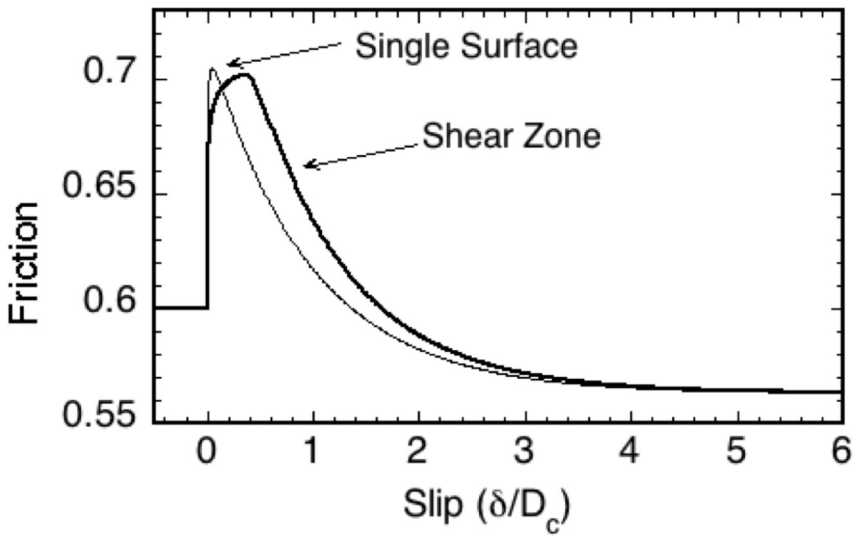

Figure 9. Results form the model runs showing friction as a function of slip. For comparison, the intrinsic frictional response for a single surface is shown together with the frictional response of the shear zone. Note that the shear zone exhibits a prolonged phase of hardening, associated with the rate/state friction response of each layer, followed by weakening. See Table 1 for parameter values.

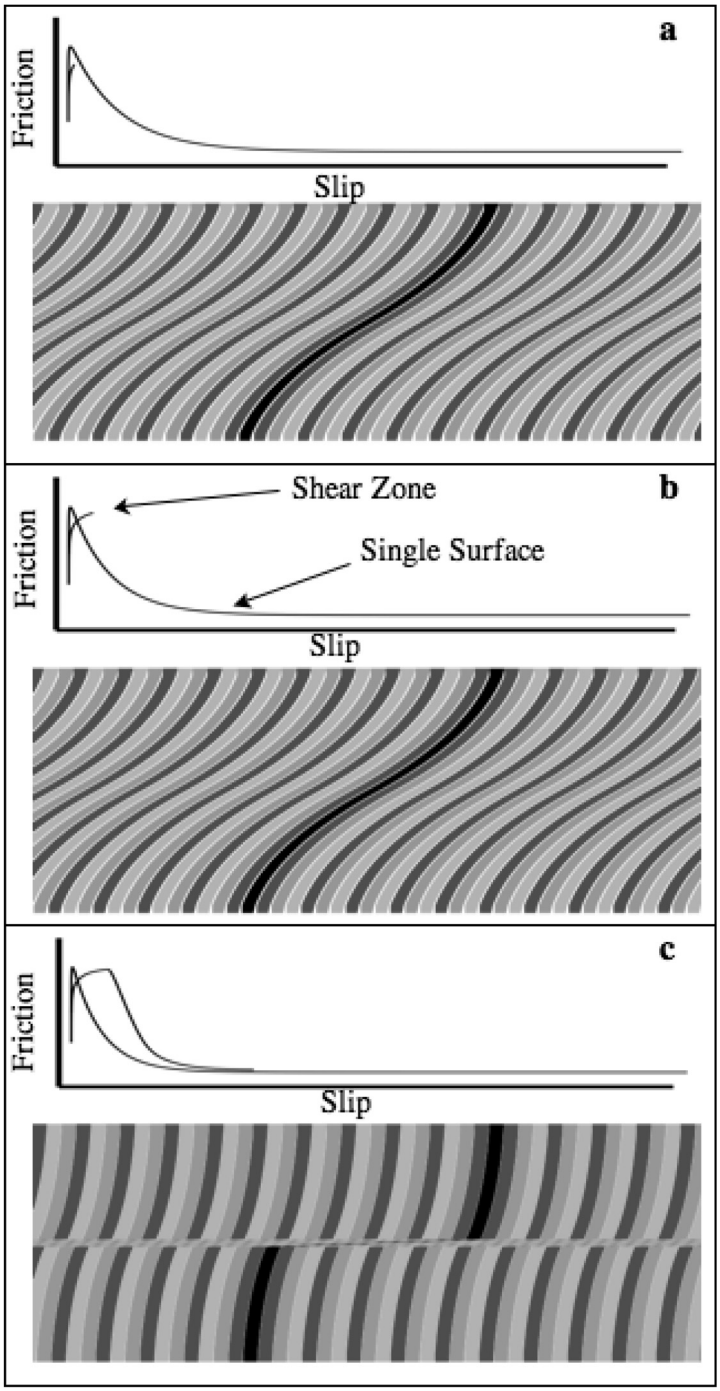

Figure 10. Three snap shots of the relation between frictional behavior and slip distribution within a model fault zone. In each case the response of a single surface is plotted together with the behavior for the complete shear zone. The single surface is the same in each panel. The shear zone response in panels a–c is shown for progressively greater boundary shear. Images below each plot show slip distribution, via offset of markers that were initially vertical in this orientation. Note that strain is initially pervasive but that localization occurs abruptly during frictional weakening. See Table 1 for parameter values.

the complete behavior. The panels of Figure 10 show three different amounts of shear applied at the boundary and below each plot is the spatial distribution of slip across the full shear zone.

The frictional model indicates that a perturbation in slip rate at the shear zone boundary results first in pervasive shear, up to a point, followed by localization along a single surface (Fig. 10). Comparison of the friction curves and slip distribution shows that localization occurs at the point that frictional weakening begins. The initial period of hardening, dictated by the friction rate parameter a, is prolonged in the shear zone, compared to a single surface, because each surface must proceed through this hardening phase before the zone as a whole can weaken.

4 DISCUSSION

4.1 *Shear localization and frictional behavior of granular layers*

Our observations indicate that the critical slip distance for friction of granular materials represents the combined effect of multiple particle-particle contact interfaces. This is evident in the laboratory data on shear localization (Fig. 2) showing that dilation is confined to a fraction of the layer once shear becomes localized. Laboratory data for granular layers also show evidence of localization in the form of the critical slip distance for friction D_c (Fig. 5). Our data show that laboratory measurements of D_c represent the effective critical slip distance for the zone of active shear, which points the way toward a model for upscaling laboratory results to tectonic faults. Indeed, these laboratory data are one of the motivations for the numerical model presented here.

4.2 *Spatio-temporal complexity of shear localization and delocalization*

One of the enduring puzzles of shear localization in granular fault zones is that of shear band migration and delocalization. A typical fault zone in nature, and in the laboratory, includes multiple zones of shear localization, rather than a single zone. This may indicate a progressive process of localization, where one type of feature is active for a limited time and then another takes over. Or, it may indicate that a set of shear zones operate simultaneously, to produce a penetrative shear fabric. However, in either case, the existence of multiple slip surfaces raises a fundamental question: why does shear concentrate in one location and then switch locations? Is there a strain hardening process that begins once a shear band forms and, if so, does each shear band accommodate the same critical strain prior to abandonment? Another possibility is that strain localization is a local process within the bulk, and a given shear band minimizes the rate of work for only a confined region. In this case, it is important to know what sets the length scale of this region.

Our experiments involve simultaneous shear and comminution of granular materials. Previous works have documented the relationship between comminution and strain under conditions similar to ours (e.g., Mandl et al., 1977, Marone & Scholz 1989). Although our experiments include detailed measurements of macroscopic stress and layer strain, these data are of limited value in answering the most important questions raised above. One would like to have independent assessment of the spatial distribution of shear strain as a function of imposed shear on the layer. While this is beyond the scope of the present data, our measurements of layer dilation as a proxy for shear localization offer some information, and the numerical model provides some insight about how the intrinsic frictional response of surfaces within a zone effect the overall response of a fault zone.

5 CONCLUSIONS

Laboratory friction experiments combined with constitutive modeling provide a powerful means of investigating problems in shear localization. Our laboratory data show that layer dilation, in response to small perturbations in creep stress rate or strain rate, can be used as a sensitive proxy for the degree of strain localization. For granular layers sheared at normal stresses up to a few MPa, shear strain becomes fully localized prior to engineering shear strains of 1. Thin section analysis

shows that shear localization is a progressive, rather than abrupt, process within a granular layer. Our experiments included velocity step tests, which probe the friction constitutive behavior and its relation to shear localization. We present a numerical model for shear within fault zones composed of multiple slip surfaces and use the model to evaluate shear localization. The spatial distribution of fault zone shear depends strongly on the intrinsic frictional properties of the materials and on elasto-frictional interaction. The model shear distribution is strikingly similar to the slip distribution documented in thin sections from experiment. Frictional processes determine the onset of strain localization and the width of active shear strain in granular shear zones. Our work has important implications for a range of conditions relevant to earthquake faulting and landslides

ACKNOWLEDGMENTS

We thank Y.H. Hatzor and the other organizers of the Batshiva de Rothschild seminar on shear physics at the meso-scale in earthquake and landslide mechanics. The workshop was extremely stimulating and very enjoyable. We gratefully acknowledge support from the National Science Foundation under grant numbers ANT-0538195. EAR-0510182, and OCE-064833. J. Samuelson, A. Niemeijer, and B. Carpenter are thanked for stimulating discussions during the course of this work.

REFERENCES

Anand, L. & Gu, C. 2000. Granular materials: constitutive equations and strain localization. *Journal of Mechanics and Physics of Solids* 48: 1701–1733, 10.1016/S0022-5096(99)00066-6.

Anthony, J.L. & Marone, C. 2005. Influence of particle characteristics on granular friction. *Journal Geophysical Research* 110(B08409): 10.1029/2004JB003399.

Beeler, N.M., Tullis, T.E. & Weeks, J.D., 1994. The roles of time and displacement in evolution effect in rock friction. *Geophysical Research Letters* 21: 1987–1990.

Bowden, F.P. & Tabor, D. 1950. *The Friction and Lubrication of Solids*. Part I. Oxford: Clarenden Press.

Chester, F.M. & Chester, J.S. 1998. Ultracataclasite structure and friction processes of the Punchbowl fault, San Andreas system, California. *Tectonophysics* 295: 199–221.

Dieterich, J.H. 1979. Modeling of rock friction: 1. Experimental results and constitutive equations. *Journal Geophysical Research* 84: 2161–2168.

Dieterich, J.H. & Kilgore, B. 1994. Direct observation of frictional contacts: new insights for state-dependent properties. *Pure Applied Geophysics* 143: 283–302.

Gajo, A., Bigoni, D. & Wood, D.M. 2004. Multiple shear band development and related instabilities in granular materials. *Journal of Mechanics and Physics of Solids.* 52: 2683–2724, 10.1016/j.jmps.2004.05.010.

Karner, S.L., Chester, F.M. & Chester, J.S. 2005. Towards a general state-variable constitutive relation to describe granular deformation. *Earth and Planetary Science Letters* 237: 940–950, 10.1016/j.epsl.2005.06.056.

Lade, P.V. 2002. Instability, shear banding, and failure in granular materials. *International Journal of Solids and Structures* 39: 3337–3357.

Logan, J.M., Friedman, M., Higgs, N., Dengo, C. & Shimamoto, T. 1979. Experimental studies of simulated gouge and their application to studies of natural fault zones, Analyses of Actual Fault Zones in Bedrock. *U.S. Geol. Surv. Open File Rep.* 1239: 305–43.

Mair, K. & Marone, C. 1999. Friction of simulated fault gouge for a wide range of velocities and normal stresses. *Journal Geophysical Research* 104: 28, 899–28, 914.

Mandl, G., de Jong, N.L.J. & Maltha, A. 1977. Shear zones in granular material, an experimental study of their structure and mechanical genesis, *Rock Mech*., 9, 95–144.

Marone, C. 1998. Laboratory-derived friction laws and their application to seismic faulting. *Annual Reviews of Earth & Planetary Science* 26: 643–696.

Marone, C., Cocco, M., Richardson, E. & Tinti, E. 2009. The critical slip distance for seismic and aseismic fault zones of finite width. In E. Fukuyama (ed.) *Fault-zone Properties and Earthquake Rupture Dynamics, International Geophysics Series* 94: 135–162, Elsevier.

Marone, C., Hobbs, B.E. & Ord, A. 1992. Coulomb constitutive laws for friction: contrasts in frictional behavior for distributed and localized shear. *Pure and Applied Geophysics.* 139: 195–214.

Marone, C. & Kilgore, B. 1993. Scaling of the critical slip distance for seismic faulting with shear strain in fault zones. *Nature* 362: 618–621.

Marone, C., Raleigh, C.B. & Scholz, C.H. 1990. Frictional behavior and constitutive modeling of simulated fault gouge. *Journal Geophysical Research* 95: 7007–7025.

Marone, C. & Scholz, C.H. 1989. Particle-size distribution and microstructures within simulated fault gouge. *Journal of Structural Geology* 11: 799–814.

Perfettini, H. & Avouac, J.-P. 2004. Stress transfer and strain rate variations during the seismic cycle. *Journal Geophysical Research* 109: 10.1029/2003JB002917.

Rabinowicz, E. 1951. The nature of static and kinetic coefficients of friction. *Journal Applied Physics* 22: 1373–1379.

Rathbun, A.P., Marone, C., Alley, R.B. & Anandakrishnan, S. 2008. Laboratory study of the frictional rheology of sheared till. *Journal Geophysical Research* 113(F02020): 10.1029/2007JF000815.

Rice, J.R. 1993. Spatio-temporal complexity of slip on a fault. *Journal Geophysical Research* 98: 9885–9907.

Rice, J.R. 2006. Heating and weakening of faults during earthquake slip. *Journal Geophysical Research* 111(B05311): 10.1029/2005JB004006.

Rice, J.R. & Cocco, M. 2007. Seismic fault rheology and earthquake dynamics. In Handy, M.R., Hirth, G. & Hovius, N. (eds.), *Tectonic Faults: Agents of Change on a Dynamic Earth; Dahlem Workshop 95, Berlin, January 2005, on The Dynamics of Fault Zones*. The MIT Press: Cambridge, MA, USA.

Richefeu, V., El Youssoufi, M.S. & Radjaï, F. 2006. Shear strength properties of wet granular materials. *Physical Review E* 73: 051304, 10.1103/PhysRevE.73.051304.

Ruina, A. 1983. Slip instability and state variable friction laws. *Journal Geophysical Research* 88: 10359–10370.

Scholz, C.H. 1998. Earthquakes and friction laws. *Nature* 391: 37–42.

Sleep, N.H. 1997. Application of a unified rate and state friction theory to the mechanics of fault zones with strain localization. *Journal Geophysical Research* 102: 2875–2895.

Song, I., Elphick, S.C., Odling, N., Main, I.G. & Ngwenya, B.T. 2004. Hydromechanical behaviour of fine-grained calcilutite and fault gouge from the Aigion Fault Zone, Greece. *Comptes Rendus Geosciences* 336: 445–454, 10.1016/j.crte.2003.11.019.

Tullis, T.E. 1996. Rock friction and its implications for earthquake prediction examined via models of parkfield earthqauakes. *Proc. Natl. Acad. Sci. USA* 93: 3803–3810.

Wood, D.M. 2002. Some observations of volumetric instabilities in soils. *International Journal of Solids and Structures* 39: 3429–3449.

Ziv, A. 2007. On the nucleation of creep and the interaction between creep and seismic slip on rate- and state-dependent faults. *Geophysical Research Letters* 34: 10.1029/2007GL030337.